Skeletal Kinetics Mechanisms for Plasma-Assisted Combustion

Aurélie Bellemans,*† Nicholas Deak ‡ and Fabrizio Bisetti§

The University of Texas at Austin, Austin, TX, USA.

Universit Libre de Bruxelles, Brussels, Belgium.

The modeling of plasma-assisted combustion requires detailed kinetics mechanisms containing many species and reactions to model the non-equilibrium effects of plasma discharges on combustion chemistry. Integrating such large mechanisms into a multi-dimensional, unsteady framework demands important computing capacities due to the temporal stiffness of the non-linear dynamics, and the memory requirements associated with the high number of species. In this work, we apply Principal Component Analysis (PCA) in order to reduce the dimensionality of a well-established detailed kinetics mechanism for plasma-assisted combustion. Data are collected from a zero-dimensional two-temperature reactor model, whereby a nanosecond pulse generates a population of excited-state molecules and radicals in argon and air mixtures with hydrocarbon fuels. The data from the detailed mechanism are used to describe the evolution of the mixture based on principal components for plasma-assisted combustion simulations in argon and ethylene-air. The accuracy of the PCA-based models is compared against the detailed calculations, and their performance is found satisfactory.

Nomenclature

A	Matrix of eigenvectors
c_i	Species concentration (kmol/m^3)
$c_{v,i}$	Species specific heat at constant volume (J/kmol K).
E	Energy density (J/m^3)
n_i	Species number density (m^{-3})
q	Number of principal components
Q	Number of original variables
Q_E	Power density (J/m^{3}s)
Q_{el}	Elastic energy exchange (J/m^{3}s)
Q_{exc}	Inelastic energy exchange (J/m^{3}s)
Q_{loss}	Recombination and attachment electron energy (J/m^{3}s)
T	Gas temperature (K)
T_e	Electron temperature (K)
U	Internal energy (J/m^3),
z	Principal component
μ	Pulse timing (ns)
ρ	Density (kg/m^3)
ω_i	Species molar production rate(kmol/m^3 s)
FWHM	Full-Width-Half-Max (ns)
PCA	Principal Component Analysis

*Postdoc, Département d'Aéro-Thermo-Mécanique, 50 Av. F. Roosevelt, 1050 Bruxelles, Belgium.

†also at: Department of Aerospace Engineering, 2617 Wichita Street, Austin, TX, USA.

‡PhD Candidate, Department of Aerospace Engineering, 2617 Wichita Street, Austin, TX, USA.

§Assistant Professor, Department of Aerospace Engineering, 2617 Wichita Street, Austin, TX, USA.

I. Introduction

Plasma-enhanced combustion was proposed as an innovative technique to ensure efficient and stable operation in difficult regimes. The use of repetitive non-thermal plasma discharges allows for the efficient ignition of fuel-air mixtures through fast heating and the generation of reactive species such as radicals and excited atoms and molecules.[1,2] The main physical principle behind the kinetic enhancement of combustion chemistry by plasma discharges is the generation of high-energy, non-thermal electrons that ionize and excite the neutral molecules. As a result, ions, radicals and vibrationally and electronically excited molecules in the non-equilibrium plasma will initiate chain-branching reactions towards the ignition of fuel/air mixtures.[2–4]

Detailed kinetics mechanisms are crucial in modelling the effects of non-equilibrium plasma on combustion chemistry. Mechanisms for plasma-enhanced combustion are a combination of plasma kinetics with combustion pathways for the simulation of fuel-air mixtures.[5–8] Recent developments focused on the interaction of non-thermal electrons with neutral fuel and air species.[10] High-energy electrons create a non-thermal plasma in which the electron temperature is much higher than the temperature of heavy species. Further, the electron energy distribution function is non-Maxwellian and requires the solution of the Boltzmann equation in order to evaluate the electron transport coefficients and rate coefficients. A possible approach to modeling reactions that depend on the electron temperature is to fit the rate coefficients originating from the *ab initio* calculations to a range of electron temperatures and include them as such in the detailed mechanism. In recent literature,[11] this method was adopted to assemble a plasma-assisted combustion mechanism to study the kinetics of plasma-assisted ignition in argon and air. The resulting mechanism was validated by experiments[12–14] and used to study radical production and main reaction pathways in argon and air subject to nanosecond pulse discharges.

Despite the current advancements in computing power, multi-dimensional unsteady simulations remain a challenge for plasma-assisted combustion applications. Bottlenecks are the large number of species and reactions included in the mechanisms and the temporal stiffness of the chemical dynamics. Plasma exchanges take place within nanoseconds, while combustion processes develop over milliseconds.

Time-scale separation offers a first reduction strategy to the aforementioned problem. In such methods, the fast chemistry is projected onto the slowly varying manifold and only the latter is solved. This is the principle behind Rate-Controlled Constrained Equilibrium (RCCE)[19] reductions and its derived techniques. In plasma-assisted combustion applications, it is common to separate the discharge phase from the combustion simulation to handle the varying time-scales.[15–17]

Alternatively, detailed kinetics mechanisms can be reduced to a skeletal form by discarding unimportant species and reactions. The graph-based methods such as the Directed Relation Graph (DRG)[20] are widely adopted techniques. The chemical network is presented as a directed graph where the species are connected with an interaction coefficient to denote their influence on each other. A skeletal mechanism is obtained by discarding graph edges and nodes according to a specified graph search procedure.

Lumping techniques offer an alternative species-reduction approach. The objective is to regroup species with similar compositions and properties and solve them as a lumped pseudo-species.[21] In plasma applications, lumping techniques usually regroup the excited levels of a molecule or species into a separate energy bin.[30]

More recently, principal component analysis (PCA) was used to develop reduced-order models (ROMs) for chemically reacting flows. The idea behind this technique is to analyze correlations between variables and to define a new reduced set of basis function identified by the principal components. More specifically, principal components correspond to the directions with the largest variance in the chemical state-space. PCA was successfully applied to reduce large combustion simulations[23,24] and has been combined with Kriging and regression strategies to optimize the reduction.[25,26] Plasma applications were reduced using PCA in combination with a regression model for vibrational CO_2[27] and collisional-radiative models in argon and nitrogen plasma.[28,29]

The objective of the present study is to explore the applicability of principal component analysis to reduce detailed kinetics mechanisms for plasma-assisted combustion applications. PCA will be used to reduce a well-established mechanism[11] for plasma-assisted ignition simulations of low pressure fuel-argon and ethylene-air mixtures. This paper is structured as follows: Section II presents the reactor model and ignitions simulations. Section III explains the reduction strategy based on principal component analysis.

Reduced models for nanosecond pulse discharges in C_3H_8-O_2-Ar and C_2H_4-air are presented in Section IV. Conclusions are drawn in Section V.

II. Physical Modeling

A. Reactor model

A system of governing equations is presented to model the time evolution of a closed isochoric and adiabatic chemical reactor. A two-temperature model is adopted with T_e the temperature of the electrons and T the temperature of all other species. c_e indicates the concentration of electrons and c_i the concentration of particles other than electrons ($i \neq e$). c_e and c_i evolve according to the following ordinary differential equations,

$$\frac{dc_e}{dt} = \omega_e, \qquad \frac{dc_i}{dt} = \omega_i. \qquad i \neq e \tag{1}$$

ω_e and ω_i are the molar production rate of electrons and species i, respectively. $u_e = u_e(T_e)$ and $u_i = u_i(T)$ are the molar internal energy of the electrons and species i. The internal energy densities are $U_e = u_e c_e$ for the electrons and $U_i = u_i c_i$ for all other particles. c_{vi} is the specific heat at constant volume of species i and $c_{ve} = 3k_B/2$ for the electrons (k_B is the Boltzmann constant). The evolution equations for T and T_e are

$$\begin{aligned} \sum_{i \neq e} c_{vi} c_i \frac{dT}{dt} &= -\sum_{i \neq e} \omega_i u_i - Q_{el} - Q_{exc} - Q_{loss}, \\ c_{ve} c_e \frac{dT_e}{dt} &= -\omega_e u_e + Q_{el} + Q_{exc} + Q_{loss} + Q_E. \end{aligned} \tag{2}$$

Q_{loss} describes the energy lost by the electrons through recombination processes,

$$Q_{loss} = \sum_{k \in K} -u_e N_A q_k, \tag{3}$$

where K is the set of recombination reactions, q_k the rate coefficient for reaction k, u_e the internal energy of the electrons, and N_A the Avogadro number. Q_{exc} is the inelastic energy lost by the electrons due to ionization, dissociation and excitation processes,

$$Q_{exc} = \sum_{\ell \in L} -E_{exc,\ell} N_A q_\ell, \tag{4}$$

where L is the set of reactions involved, and $E_{exc,\ell}$ is the excitation or ionization energy. Q_{el} describes the elastic energy exchanges,

$$Q_{el} = 3k_B \left(\sum_{i \in S, i \neq e} \nu_i^{el} m_e/m_i \right) n_e (T_e - T). \tag{5}$$

m_i and m_e are the masses of species i and the electron, ν_i^{el} is the elastic collision frequency between species i and the electron. The power deposited by the discharge per unit volume, Q_E, is modeled as a Gaussian pulse,

$$Q_E(t) = \frac{E}{\sigma\sqrt{2\pi}} \exp\left(-\frac{1}{2} \frac{(t-\mu)^2}{\sigma^2} \right), \tag{6}$$

with μ the time of peak power, σ the pulse width related to the full-width-half-max FWHM $= 2\sqrt{2\ln 2}\sigma \approx 2.355\sigma$, and E the energy density of the pulse. The discharge consists of a sequence of pulses with a pulse frequency f. These parameters are chosen in accordance with experiments to result in an ignition within 10 to 100 μs of the first pulse.[14] Equations (1) and (2) are integrated with the stiff solver CVODE.[31]

B. Simulation test cases

Two well-established detailed mechanisms for plasma-assisted combustion[11] are used in this work. The first one describes a fuel-oxygen mixture with argon diluent (C_xH_y-O_2-Ar) which is valid up to propane (C_3H_8). The kinetics is described using 103 species in 876 reactions. From these 876 reactions, 30 depend solely on

Table 1: Presentation of the simulation test cases with two detailed kinetics mechanisms: C_3H_8-O_2-Ar and C_2H_4-air.

	case (A)	**case (B)**
Gas	argon	air
Number of species	103	163
Number of reactions	876	1167
Temperature, K	750	800
Pressure, atm	1	0.5
Fuel	C_3H_8	C_2H_4
Equivalence ratio	1	1
Peak power density, kW/cm^3	30	2000
FWHM, ns	5	15
Pulse frequency, kHz	-	100

the electron temperature T_e. The argon mechanism includes ionization reactions for 4 ions: Ar^+, H_2^+, N_2^+ and O_2^+. Ionized hydrocarbons are neglected in this model. The second mechanism is a 163 species fuel-air mechanism (C_xH_y-O_2) with 1167 reactions. Vibrational and electronic excitation reactions are included, with the exception of vibrational reactions for O_2. For both mechanisms, electron impact reactions are described for collisions with Ar, O_2, H_2, CH_4, C_2H_4, C_2H_2 and C_3H_8. Rate coefficients for the latter were predicted using the Boltzmann equation solver, Bolsig+, and tabulated for a large range of electron temperatures (0.1 to 100 eV) for a composition of 20% O_2 and 80 % N2. Electron momentum effects were neglected.

Both mechanisms were used to simulate two cases as described in Table 1. Case (A) presents the simulation of a single nanosecond pulse discharge in a C_3H_8-O_2 mixture diluted in argon. The mixture does not ignite. Case (B) simulates the plasma-assisted ignition of a C_2H_4-air mixture using a burst of nanosecond pulses. The conditions of case (B) are relevant to supersonic combustion.

Figure 1a shows the time evolution of the species Ar^*, O, H, OH, and O(^{1}D) during a single pulse discharge in argon as described by case (A) in Table 1. During the discharge phase, internal states of oxygen and argon are excited and important radicals are generated (O, H and OH). These reactive species will initiate chain branching an ignition may occur after several discharge pulses. Case (B) presents the plasma-assisted ignition test case of ethylene-air using multiple pulses. Each pulse produces reactive species (radicals and excited states) as can be observed in Figure 1b. The combustion products CO_2 and H_2O increase with every pulse up to the ignition of the mixture after 4 pulses at ≈ 40 μs. The time to ignite is defined as the time where the CO_2 gradient is maximum with respect to the timing of the peak discharge power during the first pulse. Figures 2a and 2b represent the time evolution of the electron temperature T_e, and the electron number density n_e for cases (A) and (B), respectively. The electron temperature varies according to the discharge. The peak electron temperatures reaches a maximum of 54,500 K in argon and 49,500 K in air. Electrons are produced and consumed with every pulse as can be seen in Fig. 2b.

III. Mechanism reduction

Principal component analysis reduces the dimensionality of large kinetic mechanisms by projecting the detailed model consisting of Q variables on a smaller truncated base consisting of $q < Q$ principal components. This new base is obtained by analyzing correlation between variables through their variance. A ROM is obtained as the number of governing equations is compressed from Q variables to a reduced number of principal components.

Training data are collected starting from high-fidelity simulations with the detailed kinetics mechanism. The time evolution of each conserved variable is sampled across the computational domain. In this application, the conserved variables correspond to the molar concentrations of the species in the detailed mechanism. The samples are collected in matrix $\mathcal{C}$, of size $[n \times Q]$ with n the number of observations or points in space

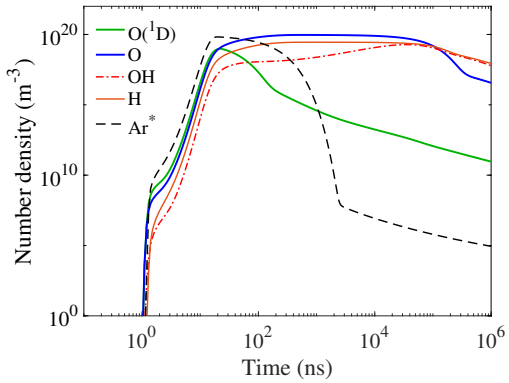

(a) Single pulse in a stoichiometric C_3H_8-O_2-Ar mixture at 750 K and 1 atm.

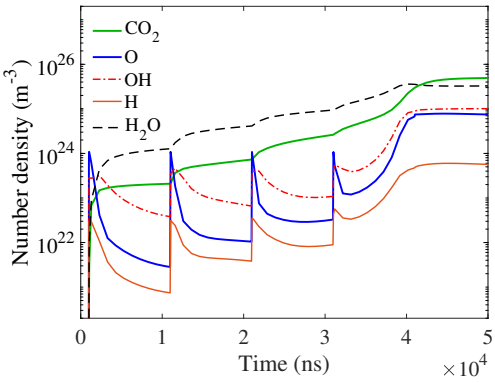

(b) Burst of pulses in a stoichiometric C_2H_4-air mixture at 800 K and 0.5 atm.

Figure 1: Time evolution of the main species and radicals in a fuel-argon and fuel-air mixture.

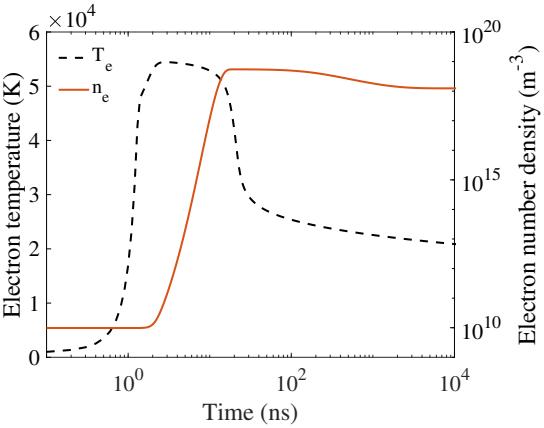

(a) Single pulse in a stoichiometric C_3H_8-O_2-Ar mixture at 750 K and 1 atm.

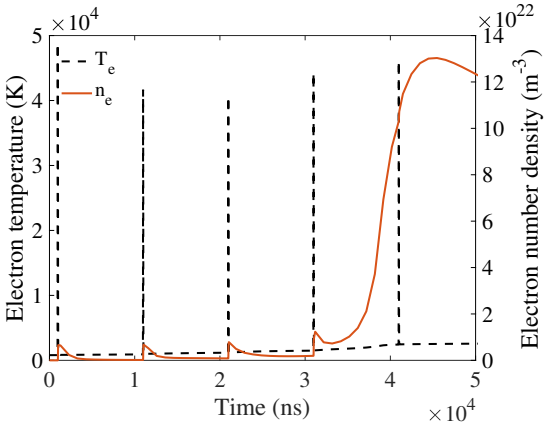

(b) Burst of pulses in a stoichiometric C_2H_4-air mixture at 800 K and 0.5 atm.

Figure 2: Time evolution of the electron temperature T_e (black dashed line) and electron number density n_e (orange line) in a fuel-argon and fuel-air mixture.

or time.

Prior to the analysis, it is essential to pre-process the data. This includes the removal of outlying observations and the scaling and centering operations. Outliers are the samples that are either very large or very small in magnitude with respect to the others. The scaling and centering operations are essential in order to compare the variables on the same scale in terms of variance. An overview of various scaling techniques with applications to reacting flows is given in Parente et al.[32] and summarized in Table 2.

Principal components are obtained through the solution of an eigenvalue problem on the covariance matrix $\mathcal{S}$, using the correlated samples in matrix $\mathcal{C}$. The matrix of eigenvectors A, resulting from the eigenvalues L in the single value decomposition, correspond to the principal components (also called scores),

$$\mathcal{S} = \frac{1}{n-1}\mathcal{C}^T\mathcal{C} = ALA^T \tag{7}$$

A reduced representation is obtained by truncating the matrix of eigenvectors A to a smaller matrix A_q containing only the variables that contain most of the variance in the system. The matrix of conserved

variables $\mathcal{C}$ is consequently projected on a new base which is made up out of the columns of A_q,

$$Z_q = \mathcal{C}A_q \tag{8}$$
$$\tilde{\mathcal{C}}_q = Z_q A_q^T \tag{9}$$

Analyzing the latter, it is clear that the principal components are a linear combination of the original variables. A reconstructed set of conserved variables $\tilde{\mathcal{C}}$ can be retrieved by inverting Eq. 8.

In practice, it is necessary to rewrite the entire state space in terms of principal components to obtain a consistent ROM. The governing equations are rewritten in terms of principal components Z, and the species production source terms are projected onto the new base,

$$\omega_Z = \omega_{\mathcal{C}} A_q. \tag{10}$$

A matrix-vector multiplication is performed every iteration in the solution process in order to retrieve the conserved variables. These variables are necessary in order to calculate the thermodynamic and kinetic evolution of the mixture. The computational cost of this operation is negligible with respect to the cost of solving the ODEs.

The principal components or scores are a linear combination of the original variables,

$$z = \sum_{j=1}^{Q} b_{ij} c_j \qquad i \in \{1, ..., q\} \tag{11}$$

with z a score or principal component and c_j the vector containing the original molar concentrations. The weights, denoted by b_{ij}, are chosen to maximize the variance within the data. Analyzing these weights for all scores contained in matrix A_q, gives insight into the reaction kinetics.

IV. Discussion

The application presented in this paper is the reduction of a detailed kinetics mechanisms for simulating nanosecond pulse discharges in fuel-argon and fuel-air mixtures. Principal component analysis is applied on high-fidelity data obtained with zero-dimensional reactor simulations. First, a model is produced *a priori* for which various pre-processing techniques are compared. An interpretation of the principal component weights is given with respect to the kinetics. The obtained reduced models are thereafter verified *a posteriori* with new simulations.

A. Nanosecond pulse discharges in argon

1. PCA-based reduced order model

High-fidelity data are collected using the 0D reactor code with the detailed kinetics model for Ar-O_2-C_3H_8. The mixture is excited using a single nanosecond pulse discharge using the conditions described in Table 1.

Table 2: Scaling techniques for data pre-processing.

Method	**Scaling variable**
auto (std)	s (standard deviation)
level	$\bar{\mathbf{y}}$ (mean value)
range	$max(\mathbf{y}) - min(\mathbf{y})$
max	$max(\mathbf{y})$
Pareto	$\sqrt{s}$
VAriable STability (vast)	$s^2/\bar{\mathbf{y}}$

Data are collected according to the integration time step of the ODE solver. More samples are collected during the discharge phase to capture fast changes in composition. The pre-processing operation removes outlying data points and centers and scales the training data. In order to detect the outliers, the distance of each realization is measured with respect to the data center using the Mahalanobis distance,

$$D_M = (\mathcal{C} - \bar{\mathcal{C}})^T \mathcal{S}^{-1} (\mathcal{C} - \bar{\mathcal{C}}), \tag{12}$$

with matrix $\bar{\mathcal{C}}$ a matrix containing the average values of the variables. Observations for with a large D_M are discarded from the set.

The centering operation centers the samples for each variable, in our case each species molar concentration c, by subtracting its average value $\bar{c}$. Next, the centered data are scaled by dividing each variable by a scaling factor s according to Table 2. An optimal scaling technique is determined by comparing the R^2 error of the reconstructed variables after PCA for a decreasing number of retained principal components q as shown in Figure 3. The error is calculated as follows,

$$R^2 = \frac{\sum(\tilde{c} - \bar{c})^2}{\sum(c - \bar{c})^2}, \tag{13}$$

with $\tilde{c}$ the reconstructed variables after PCA and $\bar{c}$ the average value of the variable.

Figure 3 compares various scaling methods for H_2O, H_2, O, C_3H_8, OH and H. The optimal technique for the main species H_2O, H_2, O and C_3H_8 is Pareto scaling. Up to 3 principal components, level scaling remains the best method for the reconstruction of the radicals OH and H. There can be concluded that all scaling methods perform in similarly up to a small amount of retained principal components. Pareto scaling shows promising results for most of the species molar concentrations analyzed.

A scree graph is used to determine the optimal amount of principal components in the ROM. In such a graph, the eigenvalue magnitude is plotted against the species index. A break between small and large eigenvalues becomes apparent, and guides the selection of the optimal number of components q. Figure 4 presents the scree graph for 4 scaling techniques. Using max scaling, we observe a break after 25 principal components. Similar results are obtained with level scaling. Using standard scaling, the number of retained components increases to 30. No break is observed using Pareto scaling. From this scree graph we can therefore conclude that the optimal amount of principal components lies around 25. This results in an *a priori* model reduction from 103 original variables to 25 principal components, resulting in a dimension reduction of 76%.

A principal component is a linear combination of the original variables, in our case the species molar concentrations (Eq. 11). The weights attributed to every variable describe the contribution of the conserved variables to each principal component. Figure 5 shows the weights for the first 4 principal components in reduced model with $q = 25$. The first principal component (PC1 in Figure 5a) shows major contributions from $O_2(a^1\Delta)$, C_3H_8, C_3H_6, C_2H_4 and H_2O. Those species directly relate to the fuel-air plasma reactions involving the oxygen metastable $O_2(a^1\Delta)$. The importance of $O_2(a^1\Delta)$ in oxygen discharges was demonstrated in previous work by Franklin.[34] The oxygen metastable species is known to have a low destruction rate and is a long-lived species as demonstrated here. The species C_3H_8, C_3H_6, C_2H_4 and H_2O clearly show the main mechanism towards the oxidation of the fuel and their break-down towards smaller hydrocarbons. Moreover, PC1 shows important contributions for the species nC_3H_7 and iC_3H_7.

The production of radicals occurs during energy deposition by the discharge pulse. In order to explore this process, principal component analysis was repeated with a special focus on the data obtained in the first 20 nanoseconds of the simulation. Most of the variance, 93%, is carried by the first principal component. This implies that the first principal component is representative of the discharge dynamics. Figure 6 shows the weights attributed to species molar fractions in the first principal component. This component clearly reflects the production of the primary radicals: Ar^*, $O(^1D)$ and $O_2(a^1\Delta)$. The most important species is

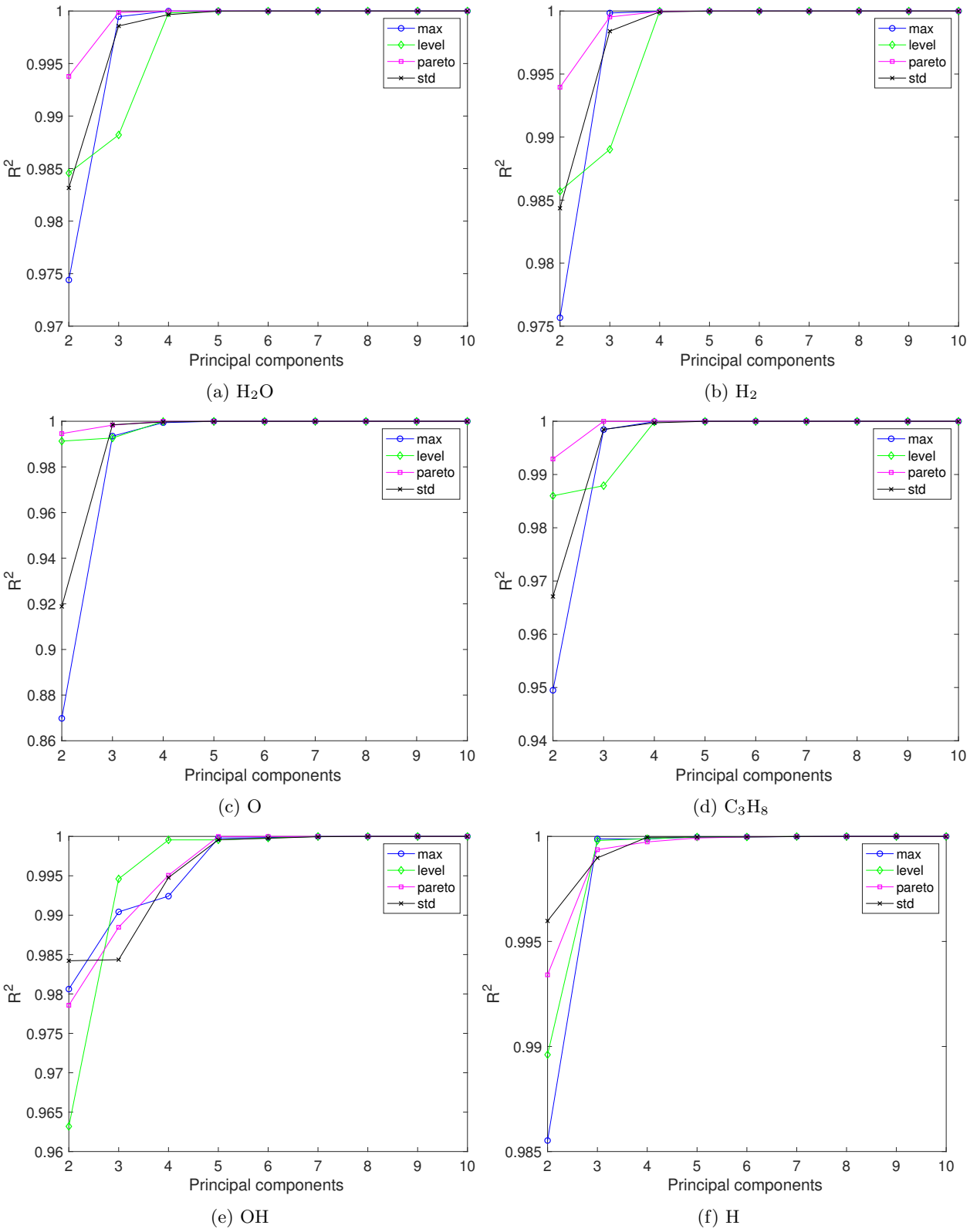

(a) H_2O (b) H_2

(c) O (d) C_3H_8

(e) OH (f) H

Figure 3: Comparison of the max, level, Pareto and standard scaling methods for the reconstruction of the species molar concentrations. R^2 error in function of the number of principal components q.

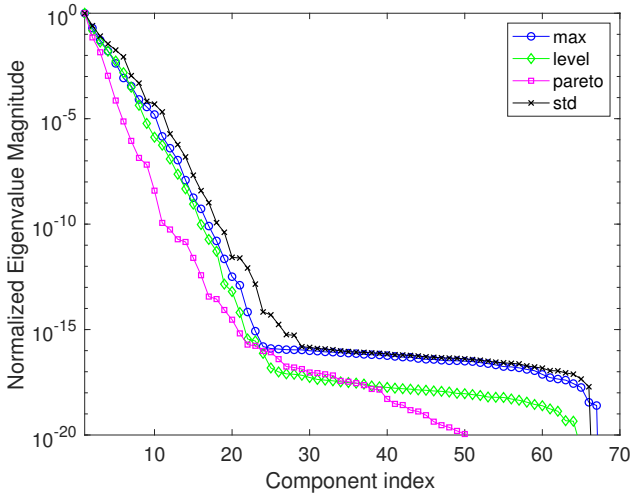

Figure 4: Normalized eigenvalues against the principal component index for various scaling methods in case (A).

the argon metastable Ar^* created by electron impact reactions and consumed by quenching,

$$e^- + Ar \rightleftharpoons Ar^* + e^-, \tag{14}$$
$$Ar^* + Ar \rightleftharpoons Ar + Ar, \tag{15}$$
$$Ar^* + Ar + Ar \rightleftharpoons Ar + Ar + Ar, \tag{16}$$

Other reactions are the electron impact dissociation of oxygen,

$$e^- + O_2 \rightleftharpoons O + O(1\,D) + e^-, \tag{17}$$
$$e^- + O_2 \rightleftharpoons 2\,O(1\,D) + e^-. \tag{18}$$

Ions are produced through the following ionization reaction,

$$e^- + Ar \rightleftharpoons Ar^+ + 2\,e^-, \tag{19}$$
$$e^- + O_2 \rightleftharpoons O_2^+ + 2\,e^-. \tag{20}$$

Small quantities of the oxygen metastable $O_2(a^1\Delta)$ are created via electron impact excitation,

$$e^- + O_2 \rightleftharpoons O_2(a^1\Delta) + e^-. \tag{21}$$

The de-excitation of the metastable form of argon results in the break-up of propane into propane as follows,

$$Ar^* + C_3H_8 \rightleftharpoons Ar + C_3H_6 + 2\,H. \tag{22}$$

2. *A posteriori analysis*

The PCA-based ROM is used in new simulations to verify its performance. The *a priori* analysis demonstrated that 25 principal components contain enough detailed information in order to represent the state-space accurately. This optimal number may vary in the *a posteriori* evaluation of the model in which the solution with the ROMs are compared to the reference solution. The number of principal components in the model was lowered to 21 in optimized simulations. The number of conserved variables was reduced from 103 species to 21 principal components. This corresponds to a dimensionality reduction of 80%. Figure 7a compares the time evolution of O, OH, H, and $O(^1D)$ between the detailed solution and the PCA model with 21 components. An accurate reconstruction was obtained ($R^2 = 0.95$ over the entire simulations).

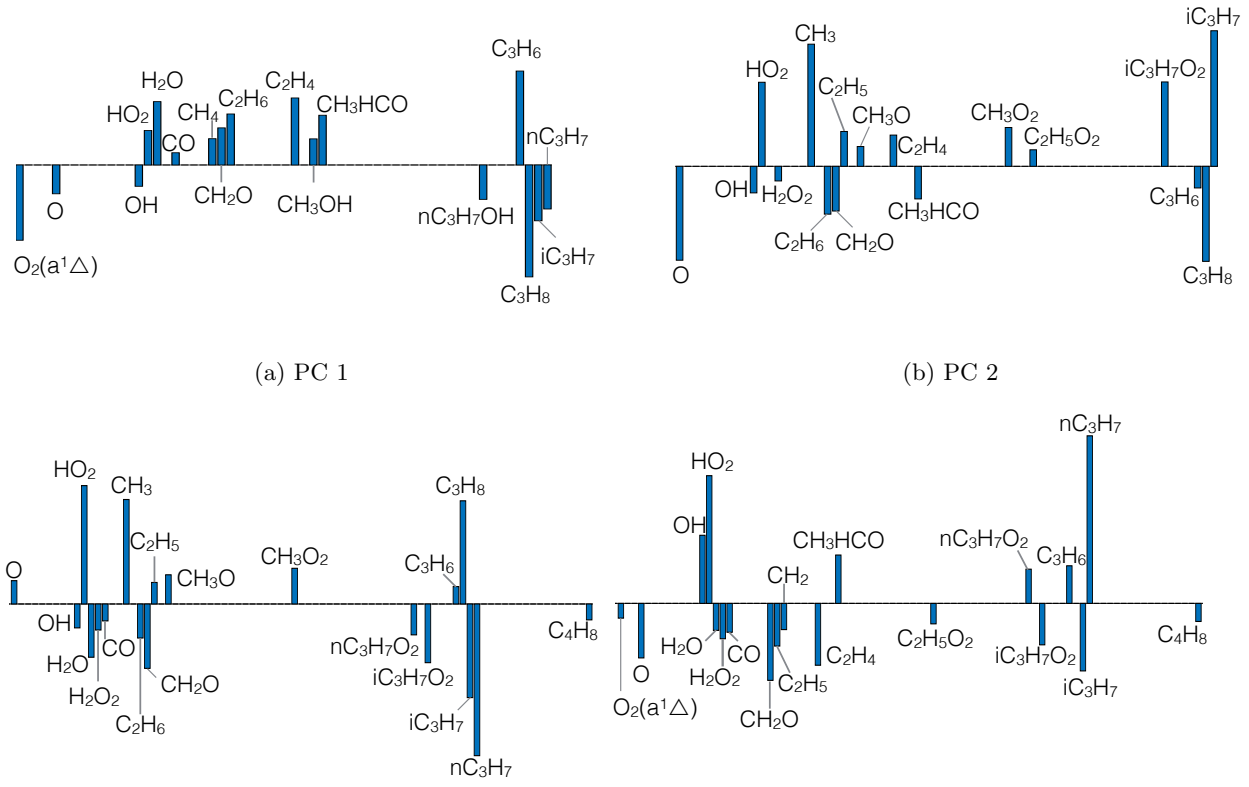

(a) PC 1

(b) PC 2

(c) PC 3

(d) PC 4

Figure 5: Principal component weights with the PCA-based model for argon at 750 K and 1 atm.

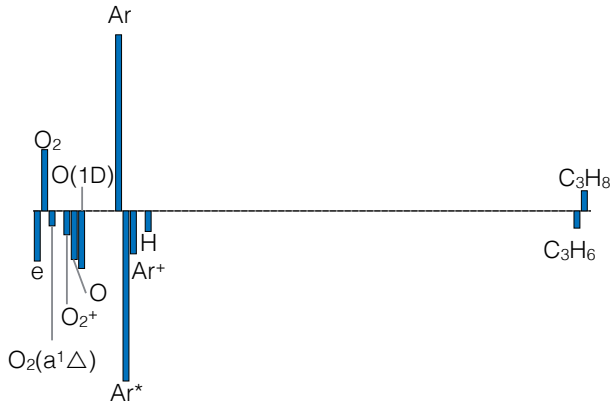

Figure 6: Principal component weights in the discharge phase for case (A).

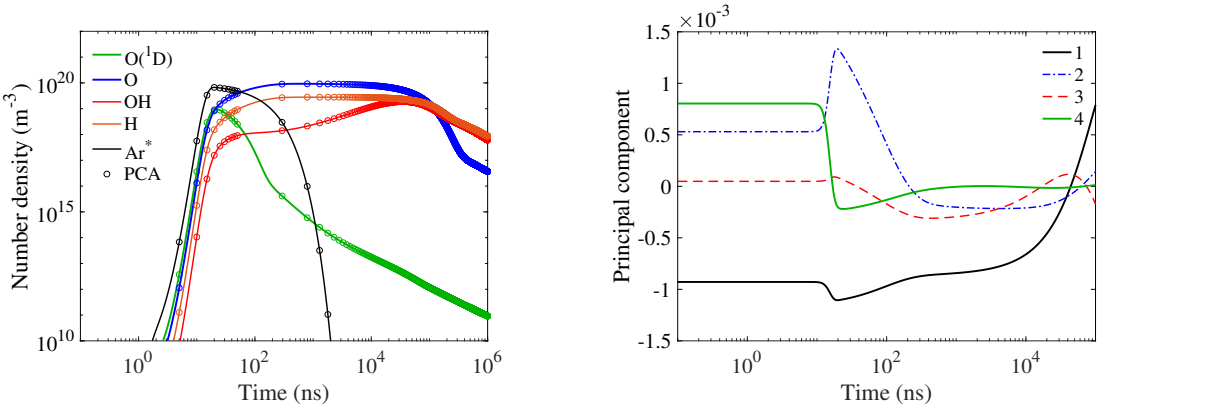

(a) Comparison of main species.

(b) Time evolution of the first 4 principal components.

Figure 7: A detailed stoichiometric C_3H_8-O_2-Ar mixture at 750 K and 1 atm (lines) was reduced to a PCA-based model with 21 components (circles).

Figure 7b represents the time evolution of the principal components over the simulation with the PCA model of 21 components. The first 4 components (full lines) carry most of the dynamical information. From the Figure can be observed that the global evolution of the system is carried in principal component 1, while components 2 and 3 model the discharge. Linking this to the weights in Figs. 5a-5d, we determine what species are important in each phase of the simulation.

The ROM was trained with data obtained for one particular reactor configuration. Next we will investigate whether the PCA model with 21 components can be used outside its training conditions. This is an important aspect to assess the applicability range of the reduced model. The input temperature will be varied from 750 to 1250 K. The pressure remains constant at 1 atm. Results were accurate using the model with 21 components. It was mandatory to increase the number of principal components to 40 in order to reproduce a correct evolution of the species in the reactor. For a smaller number of principal components, large discrepancies were observed in the species molar concentrations. Table 3 shows the R^2 error on the reproduction of O, H, OH and H_2O with the ROM of 40 principal components for initial temperatures ranging from 750 to 1250 K. The model was not able to represent reactor simulations at lower temperatures than its training temperature 750 K. Possible remedies are (1) training the PCA with a broader set of temperatures or (2) allowing a large number of principal components in the reduced model. Future work will explore different remedies to extend the applicability range of the PCA-based models.

Table 3: R^2 value for O, OH, H_2O and H obtained with 40 principal components outside the training conditions of case (A).

T [K]	**O**	**OH**	**H**	**H_2O**
750	1	1	1	1
850	0.9997	0.9985	0.9932	0.9995
950	0.9996	0.9961	0.9937	0.9065
1050	0.9991	0.9661	0.9935	0.7272
1150	0.9957	0.8861	0.9872	0.5676
1250	0.9878	0.6083	0.9714	0.4137

B. Nanosecond pulse discharges in ethylene-air

A final application of PCA is demonstrated on case (B) where we consider the plasma-assisted ignition of a stoichiometric ethylene-air mixture at 0.5 atm and 800 K using multiple nanosecond pulse discharges.

Following the same strategy, principal component analysis is applied on data obtained with the detailed mechanism. A PCA-based model is derived *a priori* and evaluated with new simulations.

1. PCA-based reduced order model

Identical pre-processing settings are used to center and scale the data. This implies that the mean value of each variable is subtracted from each observation. The performance of the scaling methods is evaluated using the scree plot in Figure 8. Again, Pareto scaling is the best technique as it can represent the total variance in the system with less principal components than the other methods. According to the scree plot in Fig. 8, 100 principal components are sufficient to describe the detailed dynamics of the reactor.

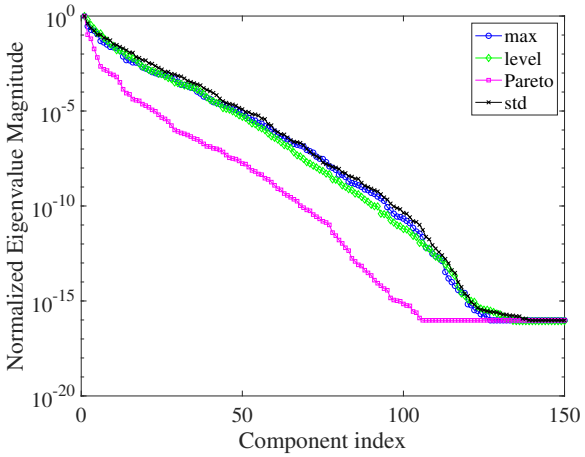

Figure 8: Normalized eigenvalues against the principal component index for various scaling methods in ethylene-air.

Figure 9 shows the weights for the first four principal components. The first principal component (Figure 9a) shows major contributions of N_2 and its first vibrational state N_2(v1). This first principal component is representative of the discharge phase. Main combustion species are represented in the second principal component (Figure 9b together with N_2(v1) and the oxygen metastable $O_2(a^1\Delta)$. The vibrational levels are well represented in the third principal component (Figure 9c). The oxygen metastables appear in the fourth principal component together with dominant contributions of HO_2 and H_2O_2 (Figure 9d).

2. A posteriori analysis

The *a priori* study presented a PCA-based model with 100 principal components for a single pulse discharge in ethylene-air. However, in the *a posteriori* simulation of the model, this number could be reduced to 80 components. Figure 10a shows a comparison between the detailed model and the model with 80 components for the time evolution of the number densities of CO_2, O, OH, H and H_2O. Excellent agreement is obtained. Perfect agreement is shown in Figure 10b where the gas temperature is compared between the detailed model and the PCA-base model with 80 components. The gas temperature increases with every pulse and thermal equilibrium is obtained at 3018 K after 40 μs.

V. Conclusion

A detailed kinetics mechanism for nanosecond pulse discharges in fuel-argon and fuel-air mixtures was reduced using principal component analysis. The C_3H_8-O_2-Ar mixture containing 103 species and 876 reactions, was reduced to 21 principal components. This corresponds to a dimension reduction of approximately 80%. Using the same strategy, a reduced model was retrieved for the plasma-assisted ignition of C_2H_4-air using 80 principal components out of 163 species. The PCA model reduces the dimensionality by 50% in this second application.

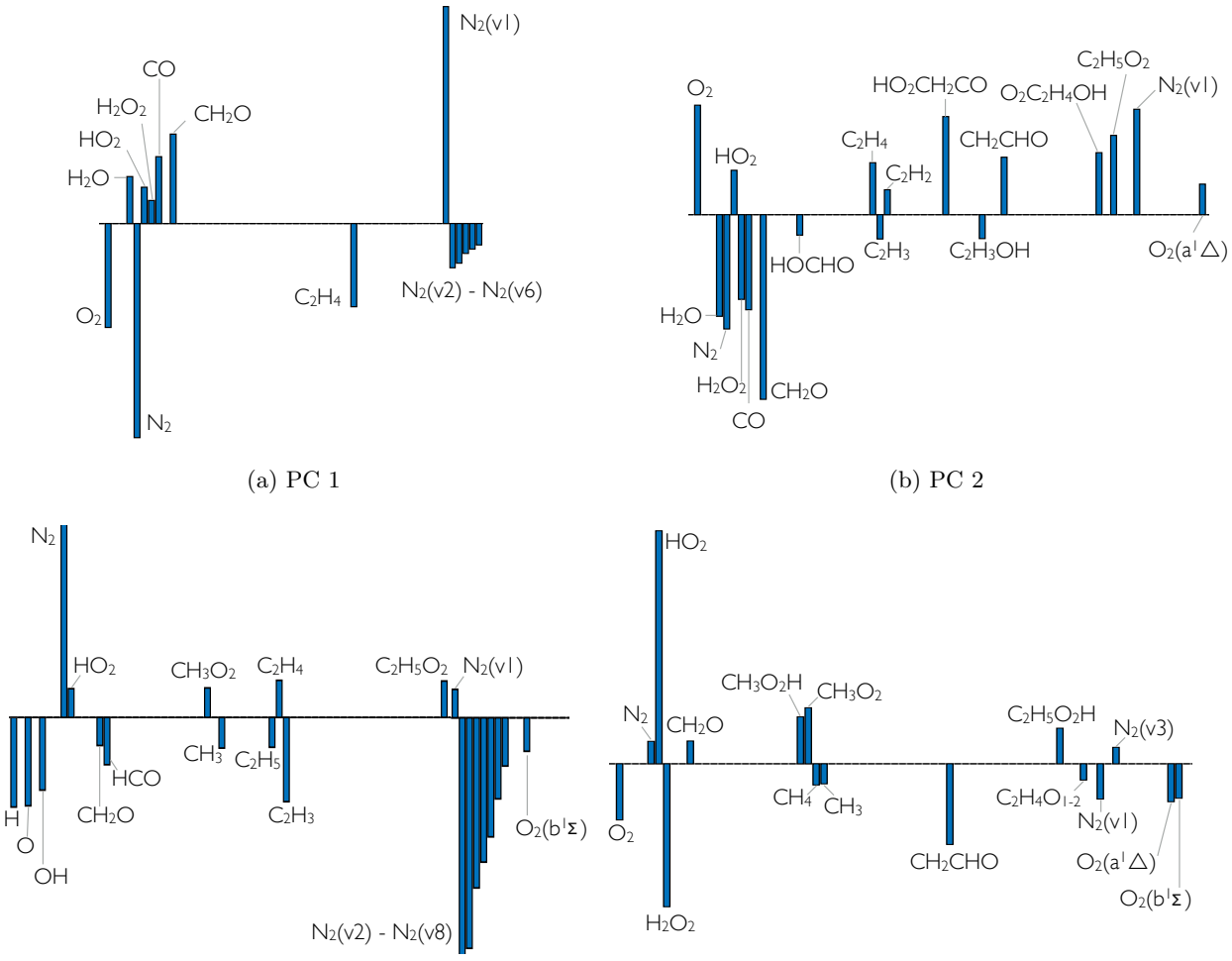

(a) PC 1

(b) PC 2

(c) PC 3

(d) PC 4

Figure 9: Principal component weights for the reduced air model at 800 K and 0.5 atm using Pareto scaling.

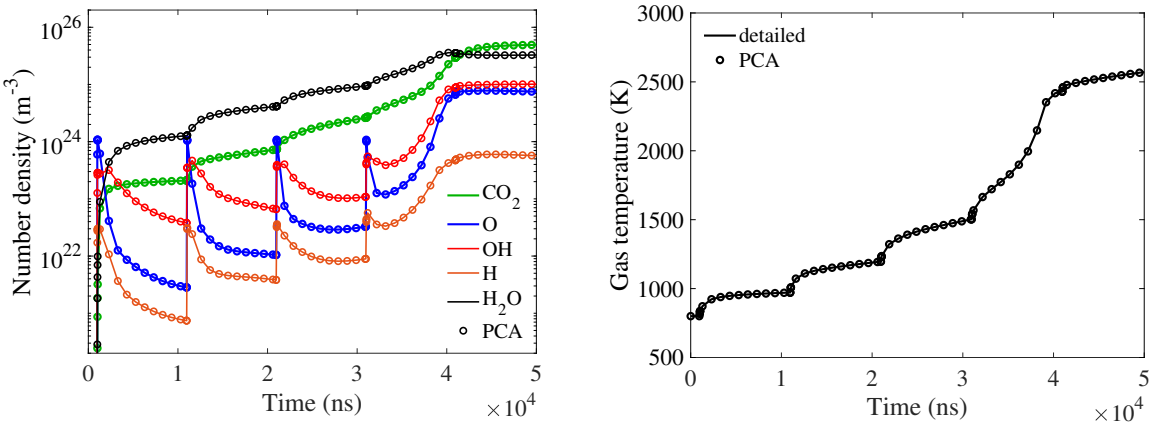

(a) Main species.

(b) Gas temperature.

Figure 10: Time evolution of the main species and gas temperature comparing the detailed model (lines) against the PCA-based model (circles) in stoichiometric ethylene-air at 0.5 atm and 800 K.

Pre-processing techniques were analyzed in an *a priori* study. The new variables in the reduced mechanism, the principal components, directly relate to the original state-space as they are a linear combination of the original variables. By analyzing the contribution of each original variable to the principal components, conclusions can be drawn on key species with respect to the non-equilibrium physics.

The PCA-models were evaluated *a posteriori* with new numerical simulations. Good agreement was obtained with respect to simulations with the detailed mechanism. The reduced mechanism can be used outside its training conditions as demonstrated in a study where the inlet temperature was varied from 750 to 1250 K.

Future work will focus on extending the applicability of the PCA-based models to a larger range of reactor conditions.

Acknowledgments

Aurélie Bellemans was supported by a fellowship of the Belgian American Educational Foundation and the F.R.S.-FNRS (Belgian Fund for Research). Nicholas Deak and Fabrizio Bisetti were sponsored in part by NSF grant Nr. 1903775.

References

[1]S M Starikovskaia. Plasma assisted ignition and combustion. *J. Phys. D: Appl. Phys.*, 39(16):265, 2006.

[2]A Y Starikovskii, N B Anikin, I N Kosarev, E I Mintoussov, M M Nudnova, A E Rakitin, D V Roupassov, S M Starikovskaia, and V P Zhukov. Nanosecond-pulsed discharges for plasma-assisted combustion and aerodynamics. *J. Propul. Power*, 24(6):1182–1197, 2008.

[3]S M Starikovskaia. Plasma-assisted ignition and combustion: nanosecond discharges and development of kinetic mechanisms. *J. Phys. D: Appl. Phys.*, 47(35):353001, 2014.

[4]Y Ju and W Sun. Plasma assisted combustion: Dynamics and chemistry. *Prog. Energy Combust. Sci.*, 48:21–83, 2015.

[5]I V Adamovich, I Choi, N Jiang, J H Kim, S Keshav, W R Lempert, E Mintusov, M Nishihara, M Samimy, and M Uddi. Plasma assisted ignition and high-speed flow control: non-thermal and thermal effects. *Plasma Sources Sci. Technol.*, 18(3):034018, 2009.

[6]N Tsolas, R A Yetter, and I V Adamovich. Kinetics of plasma assisted pyrolysis and oxidation of ethylene. part 2: Kinetic modeling studies. *Combust. Flame*, 176:462–478, 2017.

[7]S M Starikovskaia, A Y Starikovskii, and D V Zatsepin. Hydrogen oxidation in a stoichiometric hydrogen-air mixture in the fast ionization wave. *Combust. Theor. Model.*, 5(1):97–129, 2001.

[8]N L Aleksandrov, S V Kindysheva, I N Kosarev, S M Starikovskaia, and A Y Starikovskii. Mechanism of ignition by non-equilibrium plasma. *Proc. Combust. Inst.*, 32(1):205–212, 2009.

[9]Z L Petrovic, S Dujko, D Maric, and G Malovic. Measurement and interpretation of swarm parameters and their application in plasma modelling. *J. Phys. D: Appl. Phys.*, 42(19):194002, 2009.

[10]I V Adamovich, T Li, and W R Lempert. Kinetic mechanism of molecular energy transfer and chemical reactions in low-temperature air-fuel plasmas. *Phil. Trans. R. Soc. A*, 373(2048):20140336, 2015.

[11]Z Eckert, N Tsolas, K Togai, A Cherhukho, R Yetter, and I V Adamovich. Kinetics of plasma-assisted oxidation of highly diluted hydrocarbon mixtures excited by a repetitive nanosecond pulse discharge. *J. Phys. D: Appl. Phys.*, 51(37):374002, 2018.

[12]K Togai, N Tsolas, and R A Yetter. Kinetic modeling and sensitivity analysis of plasma-assisted oxidation in a $H_2/O_2/Ar$ mixture. *Combust. Flame*, 164:239–249, 2016.

[13]J K Lefkowitz, M Uddi, B C Windom, G Lou, and Y Ju. In situ species diagnostics and kinetic study of plasma activated ethylene dissociation and oxidation in a low temperature flow reactor. *Proceedings of the Combustion Institute*, 35(3):3505–3512, 2015.

[14]J K Lefkowitz, P Guo, A Rousso, and Y Ju. Species and temperature measurements of methane oxidation in a nanosecond repetitively pulsed discharge. *Phil. Trans. R. Soc. A*, 373(2048):20140333, 2015.

[15]S Yang, S Nagaraja, W Sun, and V Yang. Multiscale modeling and general theory of non-equilibrium plasma-assisted ignition and combustion. *J. Phys. D: Appl. Phys.*, 50(43):433001, 2017.

[16]T A Casey, J Han, M Belhi, P G Arias, F Bisetti, H G Im, and J-Y Chen. Simulations of planar non-thermal plasma assisted ignition at atmospheric pressure. *Proc. Combust. Inst.*, 36(3):4155–4163, 2017.

[17]A C DeFilippo and J-Y Chen. Modeling plasma-assisted methane–air ignition using pre-calculated electron impact reaction rates. *Combust. Flame*, 172:38–48, 2016.

[18]M Castela, B Fiorina, A Coussement, O Gicquel, N Darabiha, and C O Laux. Modelling the impact of non-equilibrium discharges on reactive mixtures for simulations of plasma-assisted ignition in turbulent flows. *Combust. Flame*, 166:133–147, 2016.

[19]J C Keck and D Gillespie. Rate-controlled partial-equilibrium method for treating reacting gas mixtures. *Combust. Flame*, 17(2):237–241, 1971.

[20]T Lu and C K Law. A directed relation graph method for mechanism reduction. *Proc. Combust. Inst.*, 30(1):1333–1341, 2005.

[21]P Pepiot-Desjardins and H Pitsch. An automatic chemical lumping method for the reduction of large chemical kinetic mechanisms. *Combust. Theor. Model.*, 12(6):1089–1108, 2008.

[22]I Jolliffe. Principal component analysis. In *International encyclopedia of statistical science*, pages 1094–1096. Springer, 2011.

[23]A Coussement, O Gicquel, and A Parente. Mg-local-pca method for reduced order combustion modeling. *Proc. Combust. Inst.*, 34(1):1117–1123, 2013.

[24]B J Isaac, A Coussement, O Gicquel, P J Smith, and A Parente. Reduced-order pca models for chemical reacting flows. *Combust. Flame*, 161(11):2785–2800, 2014.

[25]M R Malik, B J Isaac, A Coussement, P J Smith, and A Parente. Principal component analysis coupled with nonlinear regression for chemistry reduction. *Combust. Flame*, 187:30–41, 2018.

[26]G Aversano, A Bellemans, Z Li, A Coussement, O Gicquel, and A Parente. Application of reduced-order models based on pca and kriging for the development of digital twins of reacting flow applications. *Comput. Chem. Eng.*, 121:422–441, 2019.

[27]K Peerenboom, A Parente, T Kozak, A Bogaerts, and G Degrez. Dimension reduction of non-equilibrium plasma kinetic models using principal component analysis. *Plasma Sources Sci. Technol.*, 24(2):025004, 2015.

[28]A Bellemans, A Munafo, T E Magin, G Degrez, and A Parente. Reduction of a collisional-radiative mechanism for argon plasma based on principal component analysis. *Phys. Plasma*, 22(6):062108, 2015.

[29]A Bellemans, T E Magin, A Coussement, and A Parente. Reduced-order kinetic plasma models using principal component analysis: Model formulation and manifold sensitivity. *Phys. Rev. Fluids*, 2(7):073201, 2017.

[30]A Bellemans, A Parente, and T E Magin. Principal component analysis acceleration of rovibrational coarse-grain models for internal energy excitation and dissociation. *J. Chem. Phys.*, 148(16):164107, 2018.

[31]S D Cohen, A C Hindmarsh, and P F Dubois. Cvode, a stiff/nonstiff ode solver in c. *Comput. Phys.*, 10(2):138–143, 1996.

[32]A Parente and J C Sutherland. Principal component analysis of turbulent combustion data: Data pre-processing and manifold sensitivity. *Combust. Flame*, 160(2):340–350, 2013.

[33]A Bellemans, G Aversano, A Coussement, and A Parente. Feature extraction and reduced-order modelling of nitrogen plasma models using principal component analysis. *Comput. Chem. Eng.*, 115:504–514, 2018.

[34]R N Franklin. The role of the $O_2(a^1\Delta_g)$ metastable in oxygen discharges. *J. Phys. D: Appl. Phys.*, 35(10):1094, 2002.